

CORNER FILLET AND PARTIAL RETROFIT EFFECT ON THE BEHAVIOR OF RC COLUMNS CONFINED WITH CFRP

M. E. KASSEM¹, N. F. EL.SHAFFEY² AND M. E. ABO EL.KHAIR³

ABSTRACT

This paper investigates the effect of cross section corner fillet and retrofit on the cross section partially on the behavior of RC short columns with large scale models wrapped with External Carbon Fiber Polymers (CFRP) using finite element software (ANSYS). To study the effect of cross section corner radius, twelve model have first been conducted with various aspect ratios and four corners for each cross-section aspect ratio category with a constant number of carbon fiber layers. The behavior of each aspect ratio in both axial and transverse directions were investigated, and the results demonstrate that corner radius has an important effect on the efficiency of the retrofit cross section significantly. However, the rupture of CFRP appears in the region between the beginning of corner's curvature and the middle of the curvature. Three finite element model have been built to study the effect of retrofit on the cross section partially around the four corners on the behavior of RC short columns wrapped with external CFRP. The results showed that due to the hoop tension all models failed mainly because of the cutting of the CFRP. Moreover, FRP rupture occurs at the region between the point of start curvature and center point on the curvature line.

KEYWORDS: RC columns, Finite element, Cross section aspect ratio, Corner fillet, CFRP.

1. INTRODUCTION

FRP materials effectively have been utilized to improve the capacity and deformation of circular concrete columns with geometrical configurations that enable uniform getting stressed of the fibers, ensuring that the concrete is highly effective throughout the cross section in terms of confinement. Several parameters like concrete strength, load eccentricity, fiber type and the bond between the cross section and the carbon fiber layers have an effect on the effectiveness of the confinement of RC columns

¹ Professor, Department of Structural Engineering, Faculty of Engineering, Cairo University, Giza, Egypt.

² Associate Professor, Department of Structural Engineering, Faculty of Engineering, Cairo University, Giza, Egypt.

³ M. Sc. Candidate, Department of Structural Engineering, Faculty of Engineering, Cairo University, Giza, Egypt, mahmoud.abo.s@eng-st.cu.edu.eg.

wrapped with CFRP [1-2]. While many investigations have been conducted on the behavior of FRP confined circular columns, the effectivity of confinement for square and rectangular section is significantly reduced as the confinement stress is uniform across the cross section [3-5]. In the previous studies, due to the nonuniformity of the confinement around the cross-section parameters, experimental tests have confirmed that the corner fillet enormously affects the cross-section's performance in case of noncircular sections [6-7]. In addition, many authors have studied the effect of corner fillet in case of small-scale columns, the results show that FRP performance has obviously with the corner fillet [6]. Although most of theoretical models for noncircular sections derived from circular sections models by using shape factor and how the equivalent diameter of the noncircular sections can be calculated, few models have discovered the effect of corner fillet on the performance of the cross section in case of full retrofit [1, 8].

2. RESEARCH SIGNIFICANCE

In this paper, large scale RC columns with various corners' fillet were studied for both square and rectangular cross section in comparison with theoretical models. Moreover, the effect of retrofit on the cross section partially around the cross-section corners was studied using the nonlinear finite element software (ANSYS).

3. FINITE ELEMENT ANALYSIS

3.1 Finite Element Model

3D model is built using finite element software (ANSYS Mechanical APDL V15). Selecting appropriate materials from ANSYS program library to simulate concrete, adhesive, longitudinal reinforcements, transverse stirrups, and CFRP strips [9]. Whilst Solid65 was utilized to simulate concrete and adhesive mesh because Solid65 element can resist plastic deformation, cracking in three orthogonal directions and crushing, longitudinal and transverse reinforcement were simulated using element link180 due to its ability to carry out tension and compression force. Moreover, a layered solid element, Solid185, was utilized to model carbon fiber laminates because of its

ability to withstand against plasticity, elasticity, deflection, and large strain capabilities. Furthermore, Solid186 component was utilized for supporting steel plates at the top and the bottom of each column due to the ability to resist translation in its three different directions [9].

3.1.1 De-bonding using cohesive zone model

Cohesive Zone Material Model (CZM) was utilized to allow separation between the epoxy and the concrete [9-10]. CZM has two distinct approaches which are bilinear contact behavior and bilinear interface behavior [9-10]. In this study, the bilinear contact behavior is used. The contribution of the concrete-adhesive interface was taken into consideration in the model by recognizing interface fracture energies and suitable bilinear shear stress slips curve and normal stress gap curve. The shear-slip model generally leads to an integrated mode of separation, where in the standard transition to interface is dominated by relative tangent displacement [9-10]. The pressure gap model of the tension causes a failure mode where the normal separation from the interface controls the tangent of the slip to the interface. Using de-bonding based on just one of these two models leads to ignoring the other. While TARG170 element was utilized to model the concrete surface, the adhesive surface was modeled using CONTA174 element [9-10]. In this research, cohesive zone model has been conducted using the traction and separation option with six inputs which are maximum normal contact stress (σ_{max}), contact gap at the completion of bonding (U_n^c), maximum tangential stress (τ_{max}), tangential slip at the completion of bonding (U_t^c), artificial damping coefficient (η), and an option indicator for tangential slip under compressive normal contact stress (β) [10].

3.1.1.1 Normal contact stress-gap model

The tensile resistance is assumed to be equal to the concrete tensile strength. Consequently, failure occurs when the bonding strength under stress exceeds the tensile force of the concrete. Thus, the fracture energy of the interface is supposed to be equal to the concrete fracture energy [10] as may be obtained from Eqs. (1-8) from which G_{f0} is calculated as 0.03475 N/mm.

$$\tau_t = k_t u_t (1 - d_m), MPa \quad (1)$$

$$\sigma_n = k_n u_n (1 - d_m), MPa \quad (2)$$

$$d_m = \left(\frac{\Delta_m - 1}{\Delta_m} \right) \chi \quad (3)$$

$$\Delta_m = \sqrt{\left(\frac{U_n}{U_n^-} \right)^2 + \left(\frac{U_t}{U_t^-} \right)^2} \quad (4)$$

$$\chi = \left(\frac{U_n^c}{U_n^c - U_n^-} \right) = \left(\frac{U_t^c}{U_t^c - U_t^-} \right) \quad (5)$$

$$\sigma_{max} = 0.6 \sqrt{f'_c} \quad , MPa \quad (6)$$

$$G_{cn} = G_{fo} \left(\frac{f'_c}{10} \right)^{0.7} \quad , N/mm \quad (7)$$

$$U_n^c = G_{fo} \left(\frac{\sqrt{10} f'_c}{24.3} \right)^{0.2} \quad , mm \quad (8)$$

3.1.1.2 Shear contact stress-gap model

Eqs. (9-12) present the model equations for the shear contact stress-gap model while Fig. 1 presents both the normal stress-gap and the shear stress-slip models.

$$\tau_{max} = (0.802 + 0.078\varphi) f'_c{}^{0.6} \quad (9)$$

$$G_{ct} = \frac{0.976 \varphi^{0.526} f'_c{}^{0.6}}{2} \quad (10)$$

$$U_t^c = \frac{0.976 \varphi^{0.526}}{0.802 + 0.078\varphi} \quad (11)$$

$$\varphi = \frac{\text{Groove depth} + 1 \text{ mm}}{\text{Groove width} + 2 \text{ mm}} \quad (12)$$

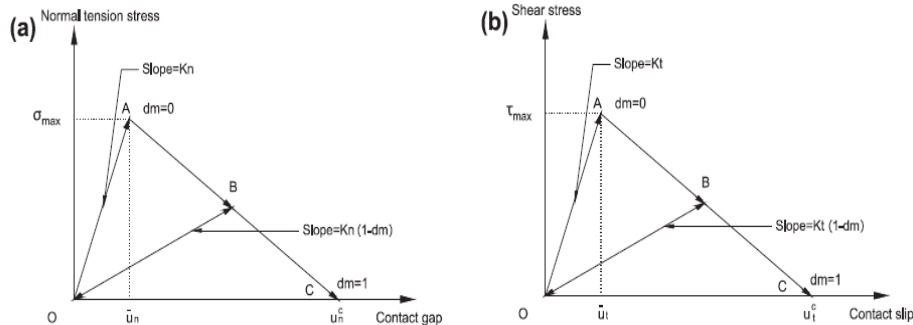


Fig. 1. (a) Normal stress – gap and (b) Shear stress – slip models [10].

4. EFFECT OF THE RADIUS OF CROSS SECTION CORNERS

To study the effect of corner radius, twelve models with four corner radiuses of the cross section are chosen 5, 10, 15, 20 mm with a constant height equals 3000 mm. The four corners were rounded to prevent premature failure and to prepare appropriate effect on column confinement. While the concrete cover is 25 mm, the concrete compressive strength is 40 MPa for all models. Four longitudinal steel bars with diameter 12 mm and 8 mm as a transverse steel bars with 100 mm spaced in the middle

and 50 mm spaced at top and bottom of each column. A combination of numbers and letters describe each model name. The first number 1.0, 1.5 and 2.0 denotes the cross-section aspect ratio, the second character is C, which refers to the column, and the third number denotes the radius of corner Table 1.

Table 1. Models configuration for radius of corners.

Model	b	T	t/b	Corner radius
1.0C5	250	250	1.00	5
1.0C10	250	250	1.00	10
1.0C15	250	250	1.00	15
1.0C20	250	250	1.00	20
1.5C5	250	375	1.50	5
1.5C10	250	375	1.50	10
1.5C15	250	375	1.50	15
1.5C20	250	375	1.50	20
2.0C5	250	500	2.00	5
2.0C10	250	500	2.00	10
2.0C15	250	500	2.00	15
2.0C20	250	500	2.00	20

4.1 Finite Element Results and Discussion

All models were analyzed under concentric load. The confined compressive strengths and strains, which have been obtained from models, are summarized in Table 2, which illustrates the stress and strain results of all models. In these results while, the lateral (tensile) strain is defined as positive, axial strain is defined as negative. In table 2, the peak stress f_{cc} and the corresponding strain ε_{cc} are equivalent to the ultimate axial stress and the corresponding axial strain at rupture failure of the CFRP wrap, respectively. Stress strain curves for square and rectangular columns with different aspect ratios 1.0, 1.5 and 2.0 are presented in Figs. 2-4. Table 2 demonstrates that the FRP efficiency depends greatly on the cross-sectional form; rectangular parts of the FRP jacket are considerably increased as opposed to square segments, and confinement efficacy decreases by raising the aspect ratio. At the same cross section aspect ratio of 1.0 and 20mm corner radius, the figure for f_{cc}/f_c was two times greater than square section with 5 mm corner radius, while the figure for f_l/f_c was 6 times greater than square section with 5 mm corner radius. On the other hand, the ratio of axial strain $\varepsilon_{cc}/\varepsilon_c$

went up by eight times and the ratio of lateral strain ϵ_l/ϵ_c went up by four times by increasing the corner radius from 5 to 20 mm

In addition, increasing in cross section ratio leads to decrease the confined strength; in case of cross section aspect ratio of 1.50 and 2.00, the strength enhancement is less than half of that in square specimen with the same corner radius Figs. 2-4. As it can be noticed from the results, corner fillets enhance the performance of concrete. However, cross section ratio has an important effect on the confinement. These figures clearly demonstrate that CFRP confinement can improve concrete performance. Moreover, corner radius is indeed a factor in determining the strength enhancement percentage [11].

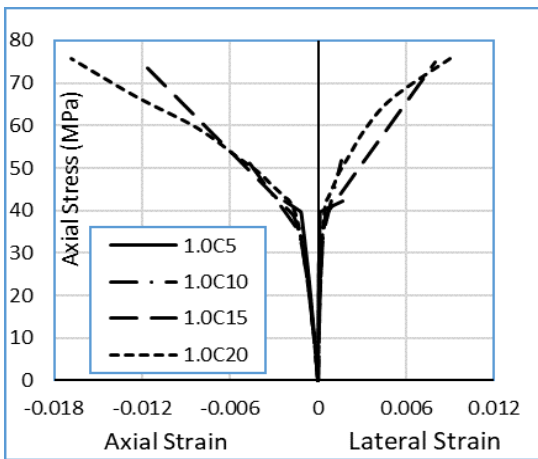


Fig. 2. Stress-strain curve for square columns ($t/b = 1.0$).

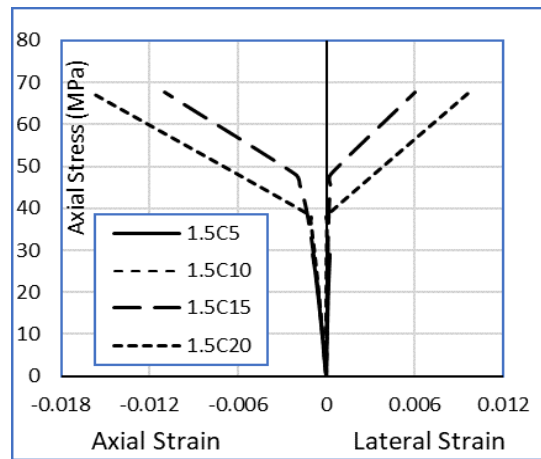


Fig. 3. Stress-strain curve for rectangular columns ($t/b = 1.5$).

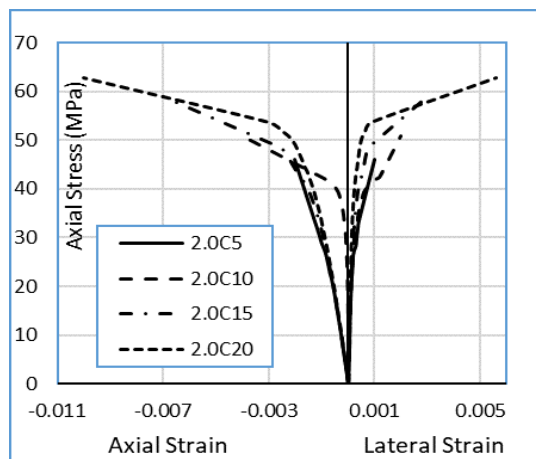


Fig. 4. Stress strain curve for rectangular columns ($t/b = 2.0$).

Table 2. Stresses and strains results.

Model	f_{cc} , MPa	f_l , MPa	f_{cc}/f_c	f_l/f_c	ϵ_{cc}	ϵ_l	ϵ_{cc}/ϵ_c	ϵ_l/ϵ_c	ϵ_{Frp}
1.0C5	42.2	11.83	1.05	0.29	0.0023	0.002	0.76	0.76	0.0017
1.0C10	51.5	15.77	1.28	0.39	0.0048	0.002	1.60	0.53	0.0025
1.0C15	74.9	38.79	1.87	0.97	0.0120	0.008	4.00	2.80	0.0079
1.0C20	75.7	40.25	1.89	1.01	0.0170	0.009	5.60	3.00	0.011
1.5C5	43.2	11.90	1.08	0.29	0.0025	0.001	0.83	0.33	0.0017
1.5C10	50.3	14.93	1.26	0.37	0.0034	0.003	1.13	1.07	0.0023
1.5C15	67.7	34.3	1.69	0.96	0.0108	0.006	3.60	1.83	0.005
1.5C20	69.7	34.3	1.74	0.86	0.013	0.007	4.33	2.33	0.009
2.0C5	46.1	11.75	1.15	0.29	0.0023	0.001	0.76	0.33	0.002
2.0C10	50.9	14.91	1.27	0.37	0.0035	0.002	1.17	0.50	0.0025
2.0C15	58.9	22.93	1.47	0.57	0.0070	0.003	2.37	1.13	0.0045
2.0C20	62.8	27.6	1.57	0.69	0.010	0.006	3.33	1.87	0.007

Table 3 illustrates CFRP strain of all models; ϵ_m is the average lateral rupture strain measured at the medium regions of each cross-sectional side, ϵ_{r1} is the average lateral rupture strain measured at the start of corner regions and, ϵ_{r2} is the average lateral rupture strain measured at the center of curvature of corner regions. Points distributed around the section perimeter where points 1, 5, 9 and 13 represent results in the center of cross section sides and 2, 4, 6, 8, 10, 12, 14 and 16 represent results in the beginning of corner radius. Furthermore, points 3, 7, 11 and 15 represent results in the center of the curvature. The distribution of CFRP strain around the entire perimeter of each module were plotted in Figs. 5-7.

Table 3. CFRP strain results around the cross section's perimeter.

Model	ϵ_m	ϵ_{r1}	ϵ_{r2}
1.0C5	0.00076	0.0015	0.0017
1.0C10	0.00110	0.0022	0.0025
1.0C15	0.00250	0.0057	0.0074
1.0C20	0.00330	0.0097	0.0109
1.5C5	0.00008	0.0014	0.0017
1.5C10	0.00097	0.0018	0.0022
1.5C15	0.00110	0.0048	0.0056
1.5C20	0.00240	0.0080	0.0091
2.0C5	0.00090	0.0013	0.0017
2.0C10	0.00120	0.0022	0.0025
2.0C15	0.00190	0.0039	0.0045
2.0C20	0.00250	0.0061	0.007

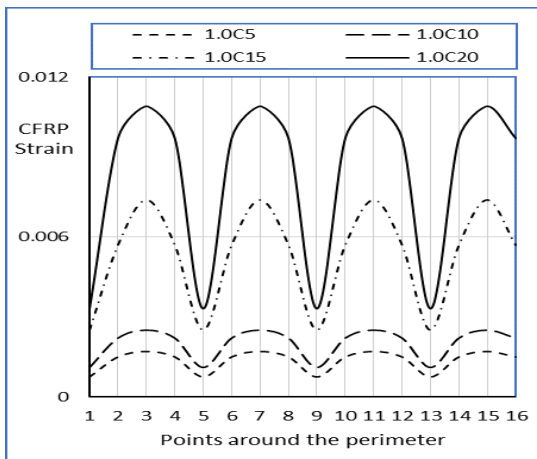


Fig. 5. CFRP strain around square column perimeter ($t/b = 1.0$).

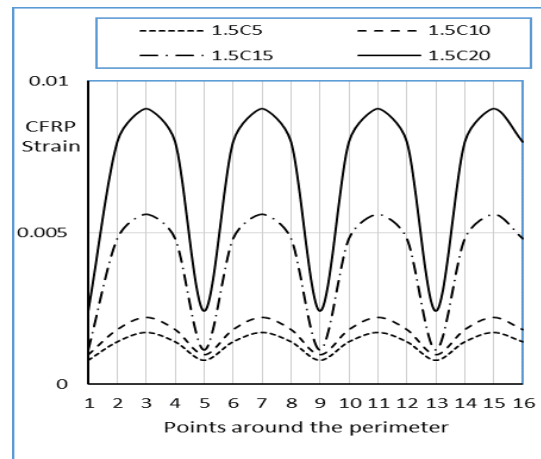


Fig. 6. CFRP strain around square column perimeter ($t/b = 1.0$).

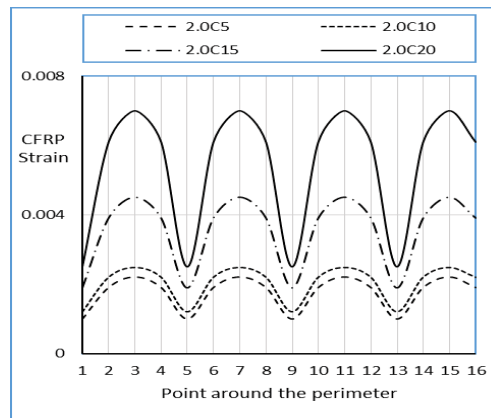


Fig. 7. CFRP strain around square column perimeter ($t/b = 2.0$).

In these figures the vertical axis represents rupture strain and the horizontal axis represents point numbers around the perimeter. It is obvious that the failure of the FRP jacket in confined segments appeared at or near the corners of the segments. Furthermore, FRP confining mechanism had the full efficiency at the corners while this efficiency reduced outside this region. On the other hand, increasing the corner radius in models with certain cross segments increased the strain concentration at corners. Moreover, in models with nearly identical r , increasing the aspect ratio decreases the FRP rupture strain as it can be seen in model 1.5C20 compared to model 2.0C20 in Table 3. Therefore, it can be concluded that the FRP rupture appears at the region between the point of start curvature and center point on the curvature line as shown in Figs. 8-19.

CORNER FILLET AND PARTIAL RETROFIT EFFECT ON THE....

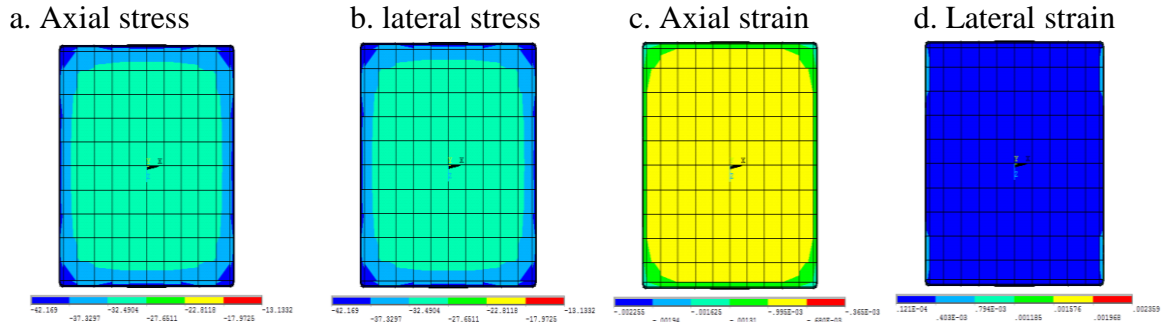


Fig. 8. 1.0C5 results.

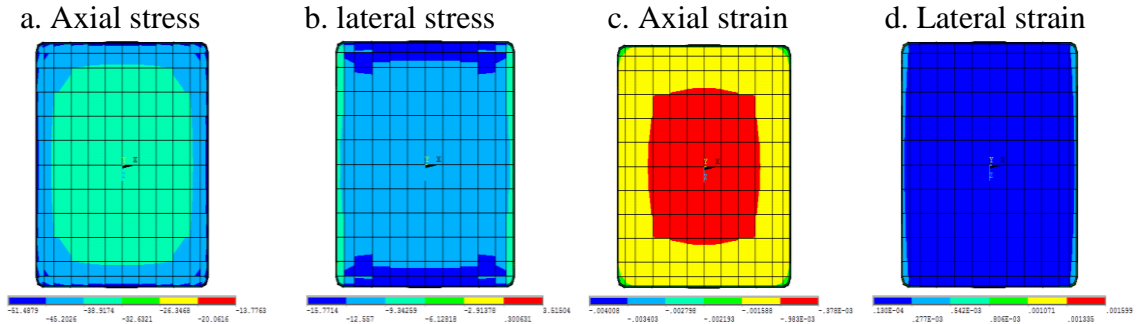


Fig. 9. 1.0C10 results.

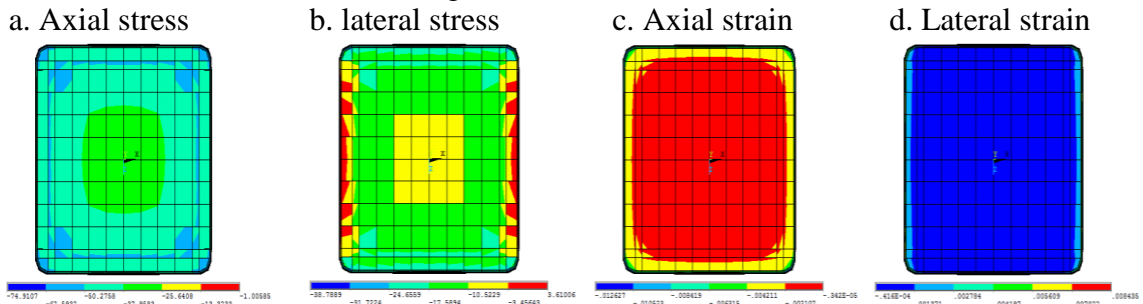


Fig. 10. 1.0C15 results.

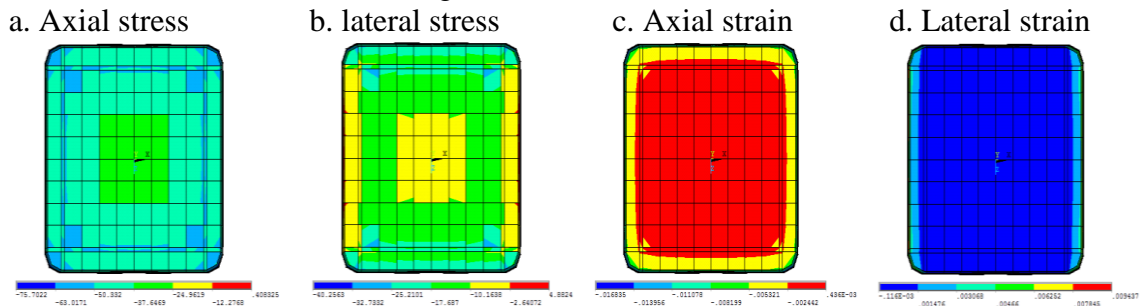


Fig. 11. 1.0C20 results.

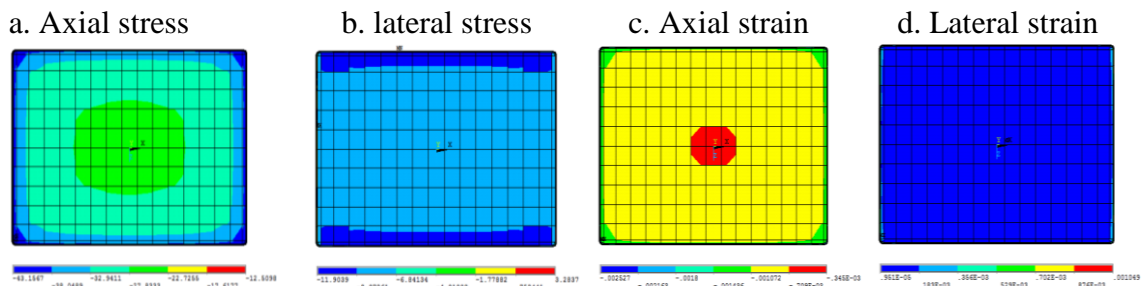


Fig. 12. 1.5C5 results.

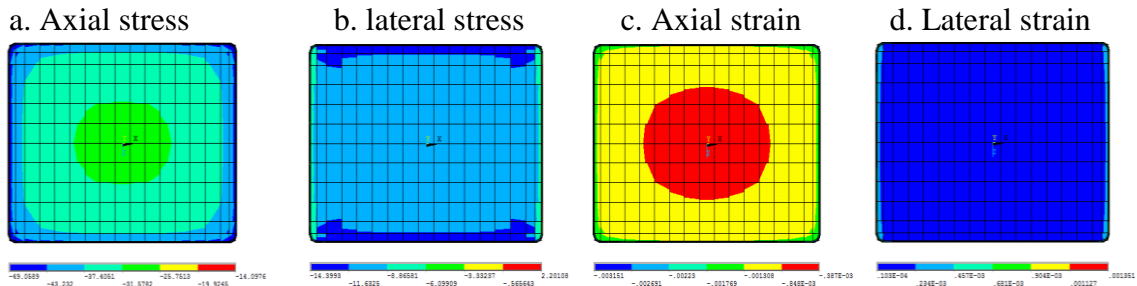


Fig. 13. 1.5C10 results.

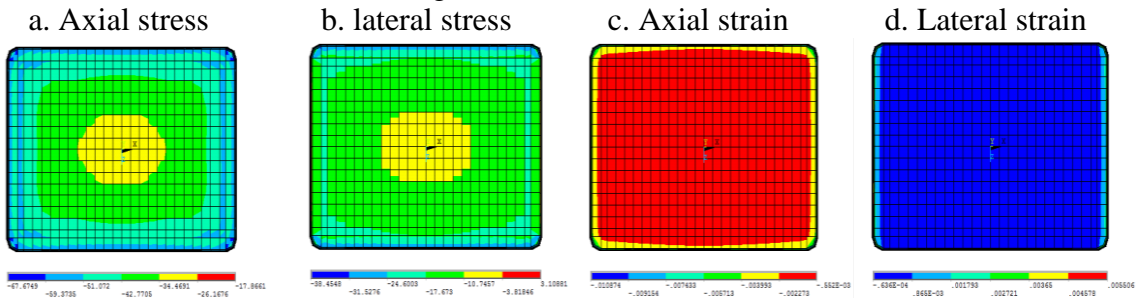


Fig. 14. 1.5C15 results.

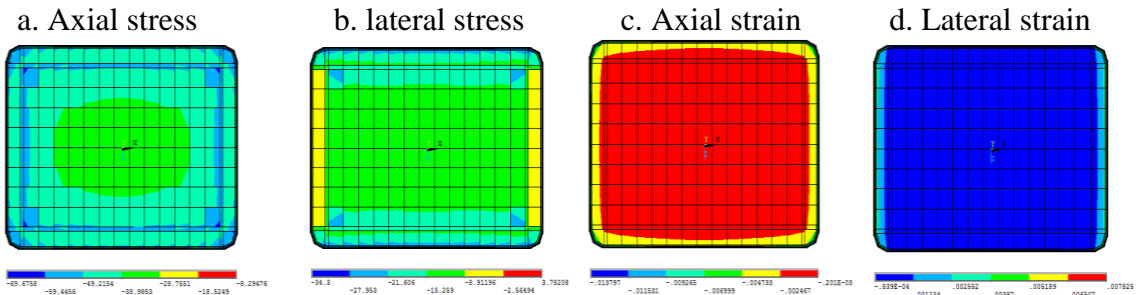


Fig. 15. 1.5C20 results.

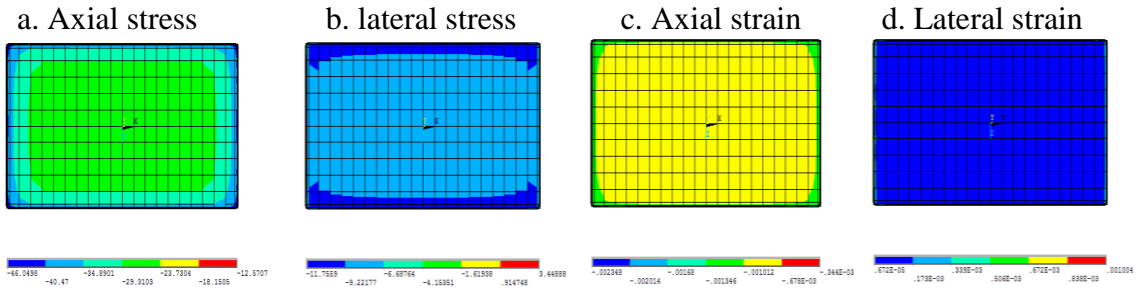


Fig. 16. 2.0C5 results.

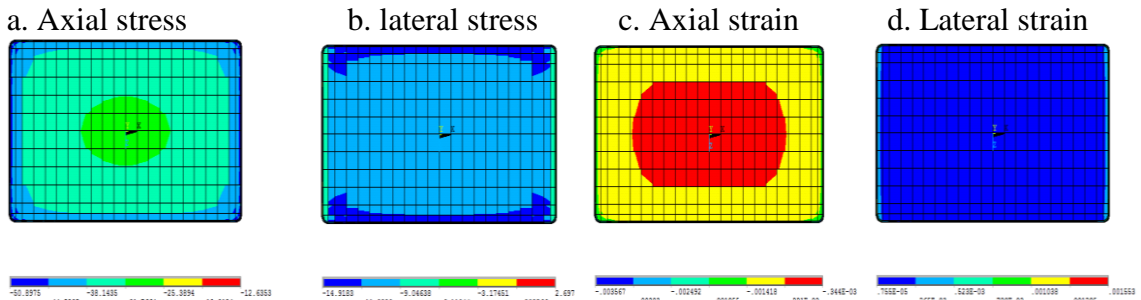


Fig. 17. 2.0C10 results.

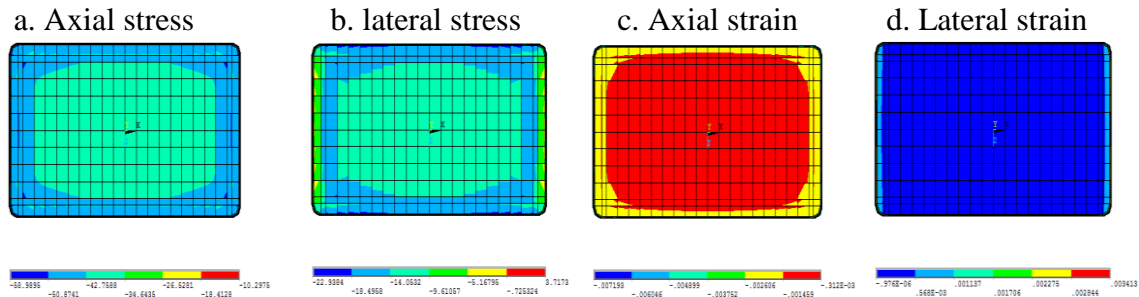


Fig.18. 2.0C15 results.

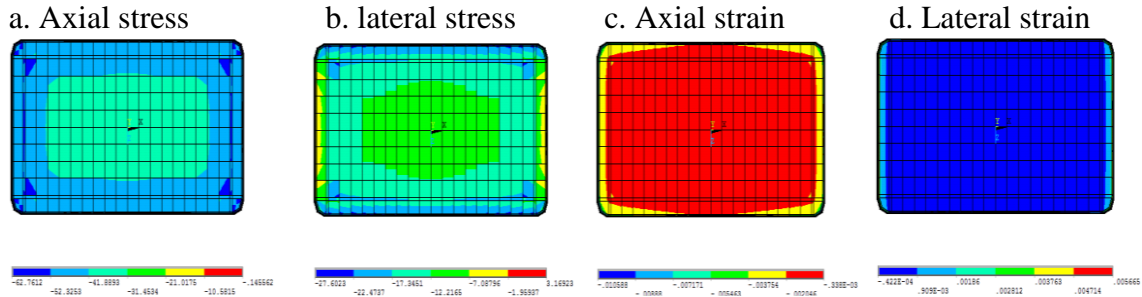


Fig. 19. 2.0C20 results.

5. EFFECT OF RETROFIT RC COLUMNS PARTIALLY

5.1 Introduction

This investigation is carried out to investigate a new method to increase the capacity of columns subjected to axial compression loads, using CFRP according to the results which have been shown in section 3. As shown in section 3, the maximum confined strain for FRP-confined members with square or rectangular section is located in the radius of corners region, therefore the failure of the section starts in this region. This technique depends on increasing CFRP layers around the four corners with a suitable overlap. Three models with 15 mm as a radius of corner with a constant height equals 3000 mm with three different cross section aspect ratio 1.0, 1.5 and 2.0. Moreover, the four corners of the models were rounded to prevent premature failure and to prepare appropriate effect on column confinement. On each side, the concrete cover was 25 mm. while the radius of each corner is 25 mm. Four longitudinal steel bars with diameter 12 mm and 8 mm as a transverse steel bars with 100 mm spaced in the middle and 50 mm spaced at top and bottom of each column. All models are rounded with 3 CFRP plies. The CFRP jacket has an elastic modulus of 225 GPa, a tensile strength of

4300 MPa and an ultimate tensile strain of 0.018; and its nominal thickness is 0.13 mm per layer.

An additional CFRP layer around each corner has been added with a suitable bond length with the other layers. Each model name is identified by a combination of numbers and letters. The first number 1.0, 1.5 and 2.0 denotes the cross section aspect ratio, the second part is EC which refers to enhanced column, and the third number denotes the radius of corner. The active bond length L_e is the length over which the majority of the bond stress is maintained as given by Eq. 13 (SI units)[1].

$$L_e = \frac{23,300}{(n_f t_f E_f)^{0.58}} \quad (13)$$

5.2 Finite Element Results and Discussion

All models were analyzed under concentric load. The confined compressive strengths and strains which were obtained from models are summarized in Table 4 which compares between stress and strain results for all models while the lateral tensile strain is defined as positive, axial strain is defined as negative. Stress strain curves of simulated square and rectangular columns with different aspect ratios 1.0, 1.5, 2.0 are shown in Figs. 20-24. There is a significant increase in f_{cc}/f_c ratio as a result of adding an additional layer of FRP around the radius of corner. At the same cross section aspect ratio of 1.0 and 15 mm corner radius, f_{cc}/f_c increased gradually from 1.87 until it reached a high of almost 2.42, while the figures show a partial growth with 1.50 and 2.0 cross section ratio reaching 1.97 and 1.72 respectively. Moreover, f_l/f_c ratio went up around two times. The ratio of axial strain $\varepsilon_{cc}/\varepsilon_c$ ratio increased significantly from 4.00 to 6.83 with cross section aspect ratio equals 1, however, there was a slight rise from 3.60 to 4.33 and from 2.37 to 2.67 with cross section aspect ratio equals 1.5 and 2.0 in a row. On the other hand, $\varepsilon_l/\varepsilon_c$ ratio went up by around one time and half. These figures clearly demonstrate that CFRP confinement can improve concrete performance. Moreover, corner radius is indeed a factor in determining the strength enhancement percentage. When it comes to CFRP strain ratio, Table 5 compares CFRP strain results for all models. ε_m is the average lateral rupture stain measured at the medium regions of each cross-sectional side, ε_{r1} is the average lateral rupture strain measured at the start

of corner regions and, ϵ_{r2} is the average lateral rupture strain measured at the center of curvature of corner regions. Due to the hoop tension all models failed mainly because of the cutting of the CFRP. This mode of failure is the most popular for CFRP confined columns however, the results proved that in most models, the FRP material tensile strength was not reached at the rupture of FRP. Furthermore, the confining mechanism is fully activated at the cross section corners while confinement exists outside these regions can be negligible. Thus, CFRP is fully activated in the region between the start point of the curve and the middle of the curve.

Table 4. Finite element results.

Model	f_{cc} (MPa)	f_l (MPa)	ϵ_{cc}	ϵ_l	f_{cc}/f_c	f_l/f_c	ϵ_{cc}/ϵ_c	ϵ_l/ϵ_c
1.0C15	74.91	38.79	0.012	0.008	1.87	0.97	4.00	2.80
1.0EC15	96.70	72.98	0.021	0.012	2.42	1.82	6.83	4.00
1.5C15	67.67	34.3	0.011	0.0055	1.69	0.90	3.60	1.83
1.5EC15	78.63	42.13	0.013	0.008	1.97	1.90	4.33	2.67
2.0C15	58.98	22.93	0.007	0.0034	1.47	0.57	2.37	1.13
2.0EC15	68.88	32.28	0.008	0.004	1.72	0.81	2.67	1.33

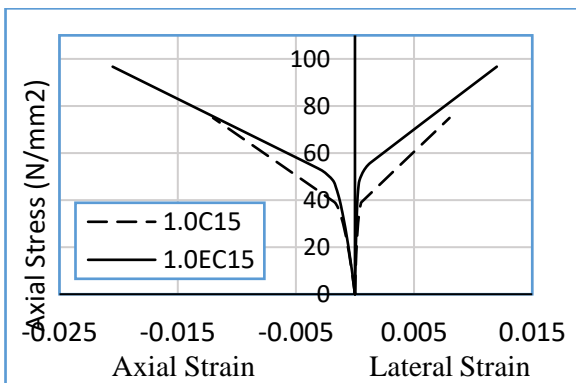


Fig. 20. Stress strain curves for column with (t/b = 1.0).

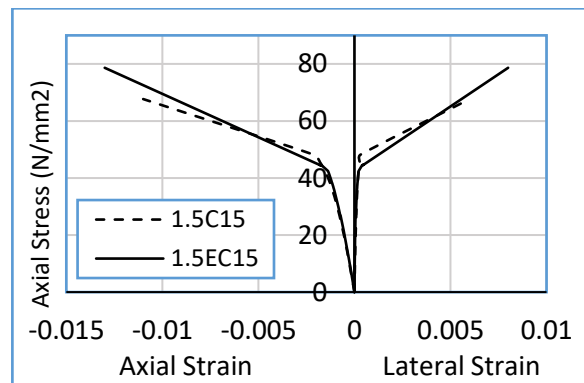


Fig. 21. Stress strain curves for column with (t/b = 1.5).

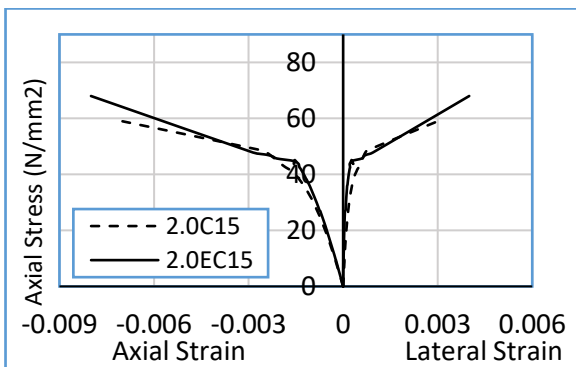


Fig. 22. Stress strain curves for column with (t/b = 2.0).

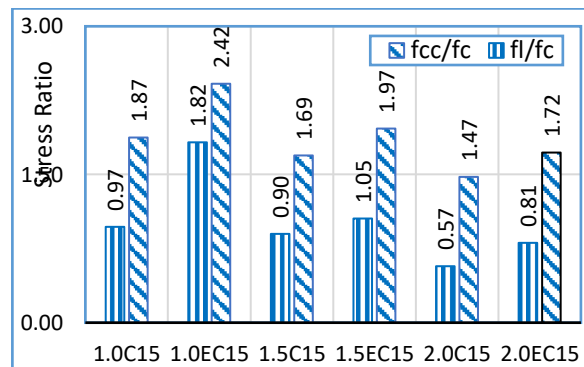


Fig. 23. Effect of additional CFRP layer on stresses ratio.

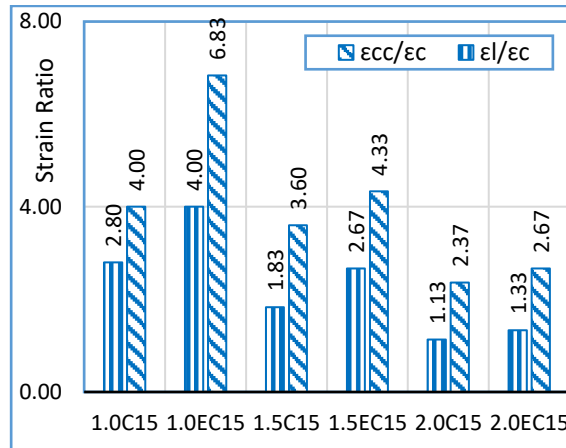


Fig. 24. Effect of additional CFRP layer on strains ratio.

Table 5 shows that the actual CFRP hoop rupture strain is not the same as rupture strain in flat coupon tests, therefore, the performance of FRP, therefore, depends largely on the cross-sectional shape. Compared to rectangular sections, FRP jackets are even more efficient in confining squares, and confinement effectiveness is reduced as the cross section ratio increases. Finite element models have indicated that the maximum strain occurs at or near the corners. Thus, the rupture of FRP takes place at the zone between the start of change in curvature and the center of corner. While the figures for carbon fiber strain fluctuated around the perimeter of the cross section, it is clear that the maximum rupture strain for carbon fiber occurs between the start and the end point of corner radius. On the other hand adding an additional carbon fiber layer around each corner has a significant enhance on the capacity of the section. Figures 25-27 illustrate enhance in carbon fiber strain around cross section perimeter and Fig. 28-30 represent finite element results which illustrate that confinement provided by the CFRP wraps is not uniform around the perimeter of the cross section for columns. The lateral strains at the corner regions were the effective at corners. Therefore, it is clear that the effective strain at failure should be based upon the average values of lateral strain at the corners. To conclude, FRP hoop rupture strains are restricted by four considerations to below the ultimate tensile strains in FRP-confined concrete from flat coupon tests: (a) the radius of corner; (b) cross section aspect ratio; (c) the effect of the overlapping length and (d) the non-uniform deformation of the concrete.

Table 5. CFRP strain results around cross section corners.

Model	ϵ_m	ϵ_{r1}	ϵ_{r2}	$\epsilon_r/\epsilon_{frp}$
1.0C15	0.0025	0.0057	0.0079	0.44
1.0EC15	0.0029	0.0069	0.0095	0.53
1.5C15	0.0011	0.0048	0.0055	0.30
1.5EC15	0.0019	0.0065	0.0074	0.41
2.0C15	0.0018	0.0039	0.0045	0.25
2.0EC15	0.002	0.0045	0.0051	0.28

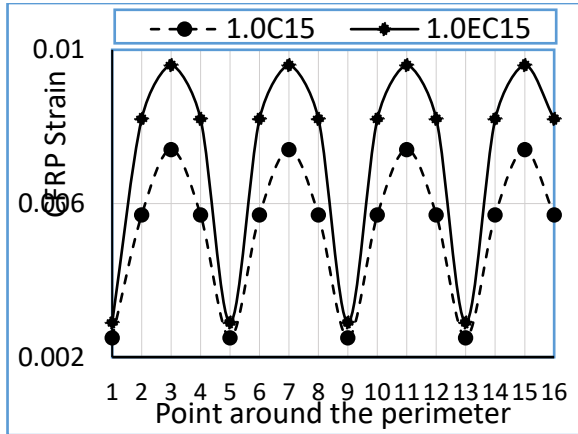


Fig. 25. CFRP strains around column perimeter for $t/b = 1.0$.

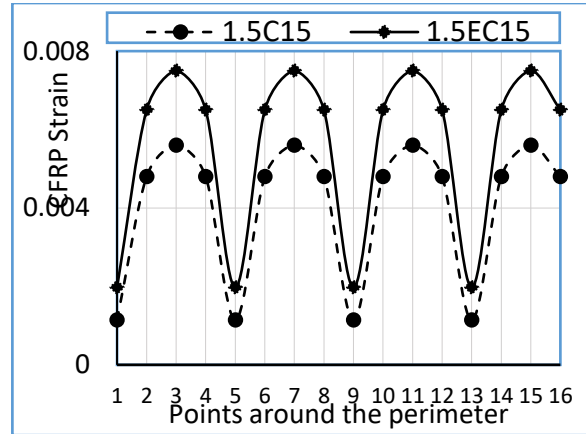


Fig. 26. CFRP strains around column perimeter for $t/b = 1.5$.

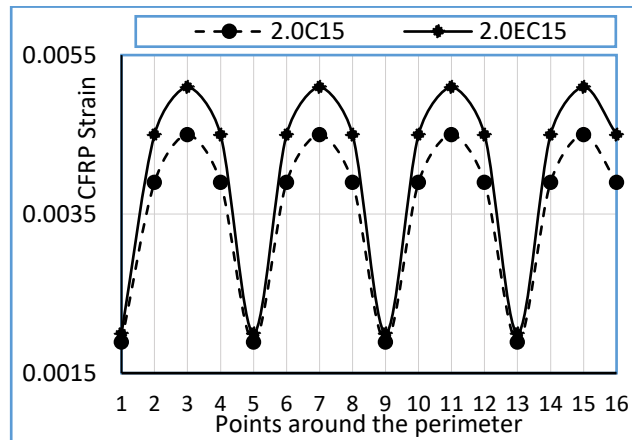


Fig. 27. CFRP strains around column perimeter for $t/b = 2.0$.

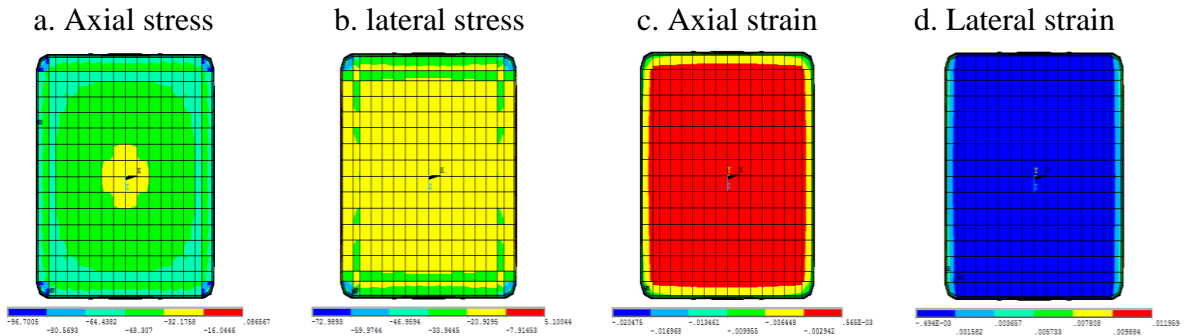


Fig. 28. 1.0EC15 results.

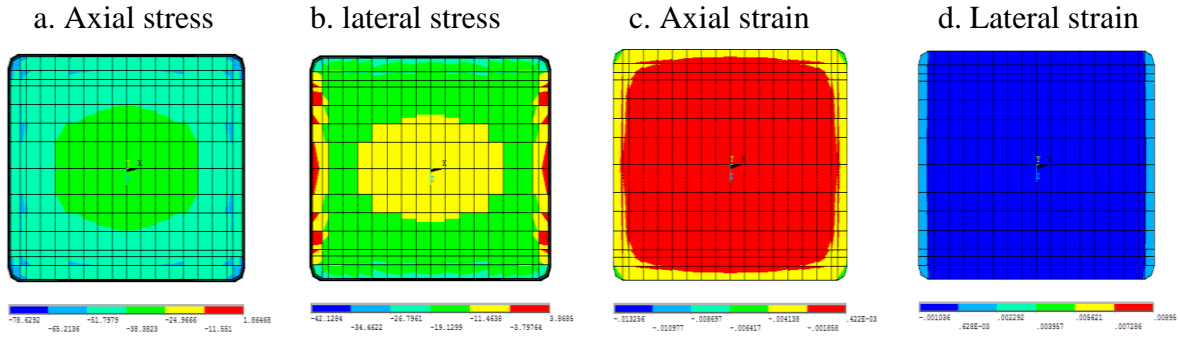


Fig. 29. 1.5EC15 results.

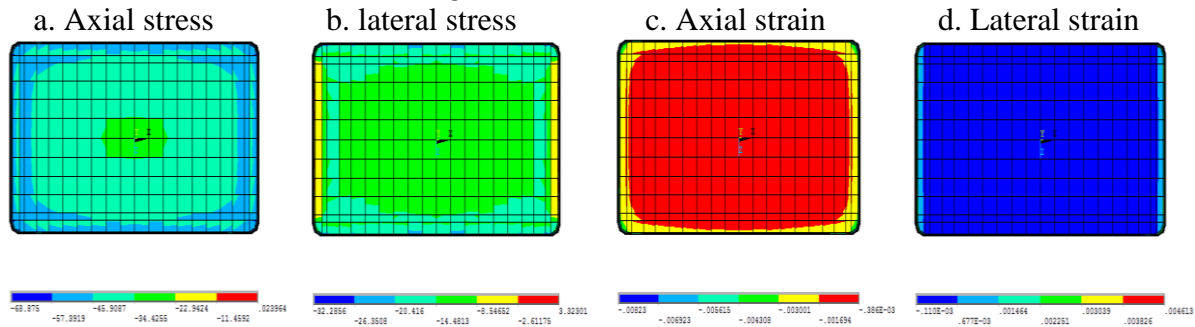


Fig. 30. 2.0EC15 results.

6. FINITE ELEMENT VERIFICATION

6.1 Finite Element Models Validation with Experimental Reference Models

Firstly, to verify the finite element modelling, three reference models were created to be compared with three tests by Xiao and Wu [12] with various carbon fiber layers. Three cylinders with a diameter of 150 mm and a height of 300 mm wrapped with one, two and three carbon fiber plies with nominal thickness 0.381 mm per layer. Whilst the concrete compressive strength was 43.8 MPa, carbon fiber modulus of elasticity, tensile strength and tensile strain were 105 GPa, 1577 MPa and 0.015 respectively. The comparison between experimental stress-strain curves and finite element reference models for each specimen are shown in Fig.. While the right curve represents the response of axial confined stress versus the axial confined strain, the left curve represents the response of the axial confined stress versus the lateral confined strain.

Secondly, finite element reference model is compared to a square column which was tested by Diego et al. [13]. This model is (150 x150) mm and 600 mm high with a corner radius of 25 mm. While the unconfined strength of concrete was 17.5 MPa, one

carbon fiber layer was wrapped the cross section with 0.3 mm thickness. Moreover, according to the manufacture, the elastic modulus and tensile strength of fibers are 242 GPa, 3,800 MPa respectively. In addition, four longitudinal steel bars with diameter 6 mm and distributed stirrups each 100 mm with 6 mm diameter. Figure 32 makes a comparison between experimental stress-strain curve for Diego et al. [13]. with the predicted one from the finite element refernece models. While the Y-axis represent the confined axial stress, the left X-axis present the lateral confined strain and the right X-axis simplify the axial confined strain. The comparison shows agreement between Diego et al. and the reference model.

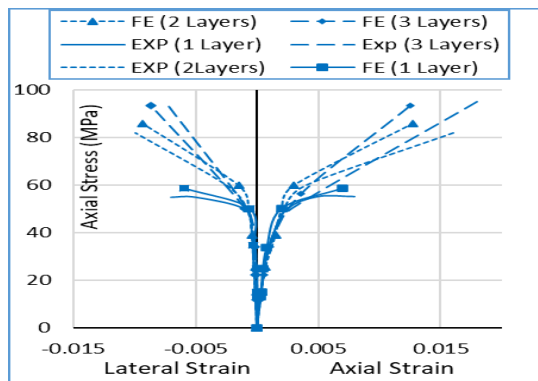


Fig. 31. Comparison of FE and experimental stress–strain curves by Xiao and Wu[12].

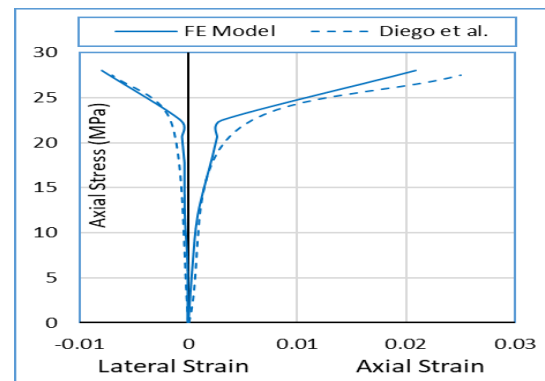


Fig. 32. Comparison of FE and experimental stress–strain curves by De Diego et al[13].

6.2 Validation of Finite Element Models with Theoretical Models

Finite element models results were verified by comparing results obtained from the FE analysis with results obtained from corresponding Tong and Hadi [4] and ACI Committee 440 2R-17 [1] as shown in Tables 6 and 7. While Hadi restrict with the round corner radius per the nominal jacket thickness should be greater than 20 ((r/t) > 20) [8].

Table 6. Estimating models for compressive strength of confined concrete column.

Author's Name	Compressive strength of confined concrete column
Hadi	$f_{cc} = 0.68f_{co} + 3.91f_l$
ACI 440 2R-2017	$f_{cc} = f_{co} + 3.3\Psi_f f_l$

Table 7. FE results compared with theoretical models.

Model	FE Results (f_{cc})	Tong and Hadi	ACI 440 2R-17
	f_{cc} (MPa)	f_{cc} (MPa)	f_{cc} (MPa)
1.0C5	42.17	-----	65.20
1.0C10	51.48	56.11	66.43
1.0C15	74.91	68.45	67.60
1.0C20	75.70	68.48	68.72
1.5C5	43.16	-----	55.25
1.5C10	50.29	60.17	56.55
1.5C15	67.67	60.19	57.81
1.5C20	69.67	60.21	59.03
2.0C5	46.05	-----	42.86
2.0C10	50.89	54.67	44.26
2.0C15	58.98	54.68	45.64
2.0C20	62.76	54.69	46.98

7. CONCLUSIONS

This paper investigates the influence of the effect of cross section corner radius and the effect of retrofit the cross section partially on the behaviour of RC columns with large scale models wrapped with external carbon fiber polymers (CFRP) using finite element software (ANSYS Mechanical APDL V15). Based on the finite element results, the following conclusions were drawn:

1. Radius of corners has an importance effect on the efficiency of FRP.
2. For the same cross section aspect ratio, the ultimate strain and the strength increase as the radius of corners increased.
3. Due to stress concentration, the axial and lateral stresses are higher at corners zone in comparison with the middle zone for each side in case of square and rectangular sections.
4. FRP confining mechanism has the full efficiency at the corners while this efficiency reduced outside this region. On the other hand, increasing the corner radius in models with certain cross segments increases the strain concentration at corners.
5. FRP rupture appears at the region between the point of start curvature and center point on the curvature line.

DECLARATION OF CONFLICT OF INTERESTS

The authors have declared no conflict of interests.

REFERENCES

1. ACI Committee 440, "Guide for the Design and Construction of Externally Bonded FRP Systems for Strengthening Concrete Structures (ACI 440.2R-17)", American Concrete Institute, Farmington Hills, 2017.
2. Mirmiran, A., Shahawy, M., Samaan, M., Echary, H. E., Mastrapa, J. C., and Pico, O., "Effect of Column Parameters on FRP-confined Concrete", *Journal of Composites for Construction*, Vol. 2, No. 4, pp. 175-185, 1998.
3. Lin, G., and Teng, J., "Three-dimensional Finite Element Analysis of FRP-Confined Circular Concrete Columns under Eccentric Loading", *Journal of Composites for Construction*, Vol. 21, No. 4, pp. 04017003, 2017.
4. Piscesa, B., Attard, M. M., and Samani, A. K., "3D Finite Element Modeling of Circular Reinforced Concrete Columns Confined with FRP Using a Plasticity Based Formulation", *Journal of Composites for Construction*, Vol. 194, pp. 478-493, 2018.
5. Gu, D. S., Wu, G. Wu, Z. S., and Wu, Y. F., "Confinement Effectiveness of FRP in Retrofitting Circular Concrete Columns Under Simulated Seismic Load", *Journal of Composites for Construction*, Vol. 14, No. 5, pp. 531-540, 2010.
6. Lam, L., and Teng, J. G., "Design-Oriented Stress-Strain Model for FRP-Confined Concrete In Rectangular Columns", *Journal of Reinforced Plastics and Composites*, Vol. 22, No. 13, pp. 1149-1186, 2003.
7. Mai, A. D., Sheikh, M. N., and Hadi, M. N. S., "Performance Evaluation of Intermittently CFRP Wrapped Square and Circularised Square Reinforced Concrete Columns under Different Loading Conditions", *Structure and Infrastructure Engineering*, Vol. 15, No. 5, pp. 696-710, 2019.
8. Thong, M. T., and Hadi, M. N. S. "Stress Prediction Model for FRP Confined Rectangular Concrete Columns with Rounded Corners", *Journal of Composites for Construction*, Vol. 18, No. 1, 2014.
9. ANSYS Mechanical APDL Manual Set, Release 14.5, ANSYS, Inc., USA, Southpointe, 2014.
10. Omran, H. Y., and El-Hacha, R., "Nonlinear 3D Finite Element Modeling of RC Beams Strengthened with Prestressed NSM-CFRP Strips", *ASCE Journal of Construction and Building Materials*, Vol. 31, No. 1, pp. 74-85, 2012.
11. Abo El.Khair, M. E., El.Shafey, N. F., and Kassem, M. E., "Strengthening of RC Short Columns with External Carbon Fiber Polymers", M.Sc. thesis, Cairo university, Egypt, 2019.
12. Xiao, Y., and Wu, H., "Compressive Behavior of Concrete Confined by Carbon Fiber Composite Jackets", *ASCE Journal of Materials in Civil Engineering*, Vol. 12, No. 2, pp. 139-146, 2012.
13. De Diego, A., Arteaga, A., Fernández, J., Perera, R., and Cisneros, D., "Behaviour of FRP Confined Concrete in Square Columns", *Materialesde ConstruCCión*; Vol. 65, No. 320, pp. 320-069, 2015.

LIST OF SYMBOLS

f'_{cc}	Confined concrete axial stress.	k_n	The normal contact stress
f'_c	Unconfined concrete axial stress.	d_m	The Debonding parameter
f'_l	Confined concrete lateral stress.	u_t	The contact slip
E_c	concrete modulus of elasticity	u_n	The contact gap
ε_{cc}	Confined concrete axial strain	U_n^-	The contact gap at the maximum normal stress
ε_c	Unconfined concrete axial strain	U_n^c	The contact gap at the completion of debonding
ε_l	Confined concrete lateral strain	U_t^-	The contact slip at the maximum shear stress
ε_{FRP}	Ultimate tensile strain for FRP	U_t^c	The contact slip at the completion of debonding
τ_t	The shear contact stress	σ_{max}	The maximum normal stress
σ_n	The normal contact stress	G_{cn}	The total value of the normal fracture energy
k_t	The shear contact stiffness	G_{fo}	The base value of fracture energy

تأثير استدارة ركن قطاع العمود والتدعيم الجزئي على سلوك الاعمدة الخرسانية المدعمة بألياف الكربون

يقدم البحث دراسة باستخدام طريقة العناصر المنتهية تأثير نصف قطر أركان القطاع وتدعيم القطاع على كفاءة العمود الخرساني المسلح المدعم خارجياً بألياف الكربون فايبر والمعرض لحمل رأسي. تم بناء اثنا عشر نموذجاً باستخدام برنامج ANSYS لدراسة تأثير تغيير قيمة نصف القطر (٥ و ١٠ و ١٥ و ٢٠ مم) على مجموعة من الأعمدة الخرسانية المربعة والمستطيلة المدعمة خارجياً بألياف الكربون فايبر. تم ملاحظة التأثير الفعال لنصف قطر أركان القطاع على كفاءة الاعمدة الخرسانية المدعمة خارجياً نتيجة تركيز الاجهادات عند اركان القطاع الأربعة ولذلك يعمل نصف قطر دوران اركان القطاع على توزيع الاجهادات بشكل منتظم بدلاً من تركيزها في هذه المنطقة. كما تم باستخدام طريقة العناصر المنتهية دراسة تأثير تدعيم القطاع بشكل جزئي حول اركان القطاع بسبب تركيز الاجهادات عند اركان القطاع مما أدى إلى تحسن وزيادة كفاءة الاعمدة الخرسانية.